Conformational change of erythroid α-spectrin at the tetramerization site upon binding β-spectrin

FEI LONG,[1] DAN MCELHENY,[1] SHAOKAI JIANG,[2,3] SUNGHYOUK PARK,[4] MICHAEL S. CAFFREY,[3] AND LESLIE W.-M. FUNG[1]

[1]Department of Chemistry, University of Illinois at Chicago, Chicago, Illinois 60607, USA
[2]Research Core Facilities, University of Missouri—Columbia, Columbia, Missouri 65211, USA
[3]Department of Biochemistry and Molecular Genetics, University of Illinois at Chicago, Chicago, Illinois 60612, USA
[4]Department of Biochemistry, College of Medicine, Inha University, Incheon 400-712, Korea

(RECEIVED July 10, 2007; FINAL REVISION August 15, 2007; ACCEPTED August 15, 2007)

Abstract

We previously determined the solution structures of the first 156 residues of human erythroid α-spectrin (SpαI-1–156, or simply Spα). Spα consists of the tetramerization site of α-spectrin and associates with a model β-spectrin protein (Spβ) with an affinity similar to that of native α- and β-spectrin. Upon αβ−complex formation, our previous results indicate that there is an increase in helicity in the complex, suggesting conformational change in either Spα or Spβ or in both. We have now used isothermal titration calorimetry, circular dichroism, static and dynamic light scattering, and solution NMR methods to investigate properties of the complex as well as the conformation of Spα in the complex. The results reveal a highly asymmetric complex, with a Perrin shape parameter of 1.23, which could correspond to a prolate ellipsoid with a major axis of about five and a minor axis of about one. We identified 12 residues, five prior to and seven following the partial domain helix in Spα that moved freely relative to the structural domain in the absence of Spβ but when in the complex moved with a mobility similar to that of the structural domain. Thus, it appears that the association with Spβ induced an unstructured-to-helical conformational transition in these residues to produce a rigid and asymmetric complex. Our findings may provide insight toward understanding different association affinities of αβ−spectrin at the tetramerization site for erythroid and non-erythroid spectrin and a possible mechanism to understand some of the clinical mutations, such as L49F of α-spectrin, which occur outside the functional partial domain region.

Keywords: erythroid spectrin; αβ-complex; tetramer; prolate ellipsoid

Reprint requests to: Leslie W.-M. Fung, Department of Chemistry, University of Illinois at Chicago, 845 West Taylor Street, MC 111, Chicago, IL 60607, USA; e-mail: lfung@uic.edu; fax: (312) 996-0431.

Abbreviations: αN-region, N-terminal region of the α-subunit; βC-region, C-terminal region of the β-subunit; CD, circular dichroism; CLEANEX-PM, phase-modulated CLEAN chemical exchange; D, translational self-diffusion coefficient; *F*, Perrin shape parameter; HSQC, 2D-heteronuclear single quantum correlation; ITC, isothermal titration calorimetry; K_d, dissociation constant; M_w, weight-average molar mass; PBS, 5 mM phosphate buffer containing 150 mM NaCl at pH 7.4; PBS6.5, 5 mM phosphate buffer containing 150 mM NaCl at pH 6.5; R_g, the radius of gyration; R_H, hydrodynamic radius; Spα, erythroid SpαI-1-156; SpαII, non-erythroid SpαII-1-147; Spβ, erythroid SpβI-1898-2083; TROSY, transverse relaxation optimized spectroscopy; [θ], mean residue ellipticity.

Article published online ahead of print. Article and publication date are at http://www.proteinscience.org/cgi/doi/10.1110/ps.073115307.

Spectrin isoforms are major proteins in the membrane (cyto)skeleton that play fundamental roles in cells (Goodman et al. 1981; Beck and Nelson 1998; Goodman 1999; Gascard and Mohandas 2000; Kordeli 2000; Bennett and Baines 2001; Beck 2005; Broderick and Winder 2005). One of the most fundamental functions of these proteins is spectrin ''self-association'': two heterodimers (αβ) associating to form a functional tetramer $(\alpha\beta)_2$ (DeSilva et al. 1992; Speicher et al. 1993). Tetramer formation involves association of the N-terminal region of the α-subunit (αN-region) with the C-terminal region of the β-subunit (βC-region) (DeSilva et al. 1992). Several hereditary hemolytic anemia diseases involve mutations in erythroid spectrin that destabilize its

tetramers, resulting in low levels of spectrin tetramers and high levels of dimers (Delaunay and Dhermy 1993). Most of the mutations occur within the proposed binding regions (the partial domains) of α- and β-spectrin. However, a few clinical mutations are outside these functional regions.

Despite the functional importance of spectrin isoforms in general, and of the tetramerization regions in particular, solution structures have not been forthcoming. This is presumably due to experimental difficulties in studying the spectrin molecule owing to its size, structural flexibility, high helical content, and the presence of stronger dimerization interactions (Begg et al. 2000; Harper et al. 2001; Bignone and Baines 2003) at the end of the α- and β-subunits opposite to the tetramerization site. We and other researchers have used recombinant proteins of spectrin fragments extensively as model systems for specific regions, such as the tetramerization regions, to study their structures and functions in spectrin (DeSilva et al. 1992; Ursitti et al. 1996; Kusunoki et al. 2004; Mehboob et al. 2005; Salomao et al. 2006). As shown in this study, even smaller spectrin fragments are difficult to study experimentally.

Based on early sequence homology studies (Speicher and Marchesi 1984) and other experimental evidence (DeSilva et al. 1992; Begg et al. 2000; Harper et al. 2001), it has long been suggested that both αN- and βC-regions of erythroid spectrin consist of partial domains, with a single helix for the αN-region and two helices for the βC-region, and that the association of these partial domains (helical bundling) leads to the formation of tetramers.

However, the only structure of the tetramerization regions that has been determined experimentally is that of the first 156-amino acid region of the erythroid α-spectrin (SpαI-1–156), which we determined by NMR methods (Park et al. 2003), showing that the partial domain consists of a helix at residues 21–45. No NMR or X-ray structure is available for the partial domain of the βC-region. Our recent spin label EPR studies show a helical conformation within the βC-region (Mehboob et al. 2005), supporting the earlier prediction of helical conformation, but the helical boundaries within the partial domain are not yet defined. Some of the experimental difficulty in studying structures of these smaller model proteins is due to their low solubility in buffers under conditions of physiological relevance.

The solution NMR structure of the recombinant protein that consists of the first 156 residues of α-spectrin shows that residues 1–20, 46–52, 82–87, 119–122, and 154–156 are in unstructured conformations. As mentioned above, residues 21–45 form the first helix (Helix C′, the partial domain), while residues 53–81 (Helix A_1), residues 88–118 (Helix B_1), and residues 123–153 (Helix C_1) form the three helices of the first triple-helical bundle structural domain (Park et al. 2003). The structure of the first domain is similar in helical lengths and in specific molecular interactions, but it is not identical to previously published structures of other structural domains from *Drosophila* (Yan et al. 1993) and chicken brain spectrin (Grum et al. 1999; Kusunoki et al. 2004). These differences may be highly significant in determining the different functions of different structural domains, or of the same domain but of different isoforms. For example, despite the sequence homology of erythroid and non-erythroid α-spectrin at the tetramerization site, their association affinities with the same β-partner (SpβI-1898–2083) are different (Mehboob et al. 2001, 2003). In general, the association affinity of non-erythroid α- and β-spectrin is much stronger than that of erythroid spectrin (Speicher et al. 1993; Ursitti et al. 1996; Begg et al. 1997; Bignone and Baines 2003).

Our previous studies have shown a 10% increase in helical content in the complex of SpβI-1898–2083 (Spβ) (Mehboob et al. 2001), yet the details of conformational change(s) are not known. (For simplicity, we will represent SpαI-1–156 as Spα and SpβI-1898–2083 as Spβ below.)

In this study, we have used circular dichroism, isothermal titration calorimetry, static and dynamic light scattering, and solution NMR methods to study the hydrodynamic properties and the dynamics/conformation of Spα in the Spα–Spβ complex. We found that, upon addition of Spβ, (1) there was a general 10%–15% increase in helicity, (2) a highly asymmetric complex was formed, and (3) ~12 residues in Spα, five residues prior to and seven residues following Helix C′ (the partial domain helix), undergo dynamic changes, presumably due to local conformational changes, from a disordered to a rigid helical conformation.

Results

Binding affinity

We measured the dissociation equilibrium constant (K_d) for the Spα–Spβ complex under the same conditions as NMR samples at pH 6.5 and 20°C and obtained an average value of 1.03 ± 0.06 μM ($n = 3$) (Fig. 1A), with an n value of 0.82 ± 0.01, a $\Delta H°$ value of −118 ± 1 kJ/mol, a $\Delta S°$ of −282 ± 4 J/mol-K, and a $\Delta G°$ of −34 ± 0.1 kJ/mol. These values are very similar to those we previously observed at pH 7.4 and 25°C (Mehboob et al. 2001).

Concentrations of free Spα in mixtures of 0.40 mM Spα and different concentrations of Spβ were calculated from this K_d value. For Spα (0.40 mM) with a 1.4 molar excess of Spβ (NMR sample conditions), only ~0.5% of Spα remained in the free state and 99.5% was associated with Spβ (Fig. 1A, inset).

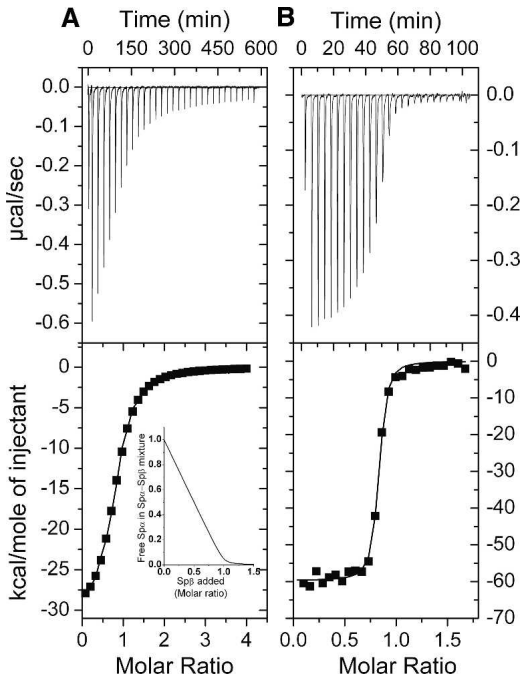

Figure 1. Isothermal titration calorimetric measurements—raw data (*top*) and fitted curve (*bottom*)—for Spα or SpαII and Spβ association. Each injection of Spα was 8 μL except for the first, which was 5 μL. Time intervals between injections were 20 min except for the first, which was 12 min. The first injection point was typically not used due to the loss of sample from the syringe needle to the sample cell. (*A*) Spα and Spβ; (*B*) SpαII and Spβ. Calculated amounts of free Spα in mixtures of Spα (0.40 mM, same as that used in NMR samples) and various amounts of Spβ, using the K_d value obtained from ITC measurements, are shown in the *inset* of *A*.

The K_d value obtained for the complex of Spβ with SpαII-1–147 was 4.2 nM ($\Delta G° = -47.7$ kJ/mol) under the same conditions, indicating a much tighter binding for the SpαII–Spβ complex than for the Spα–Spβ complex (Fig. 1B). SpαII-1–147 consists of the first 147 residues of non-erythroid α-spectrin and is highly homologous to SpαI-1–156.

Secondary structure

The $[\theta]_{222}/[\theta]_{208}$ ratio is sensitive to inter-helical interactions and has been used to distinguish between associated helices, which exhibit values ≥1, and nonassociated helices, which exhibit values ~0.8–0.9 (Mehboob et al. 2001). The average value for $[\theta]_{222}/[\theta]_{208}$ was 0.92 for Spα samples and 0.95 for Spβ samples, consistent with the presence of one nonassociated helix in Spα and two in Spβ samples at pH 6.5, similar to findings at pH 7.4 (Mehboob et al. 2001). However, the value for samples consisting of Spα–Spβ mixtures was 1.01, indicating that the pairing of the previously unpaired helices in Spα and in Spβ occurred upon complex formation, again similar to results observed at pH 7.4 (Mehboob et al. 2001).

More interestingly, the average value of $[\theta]_{222}$ at pH 6.5 was -20.3 deg·cm^2·dmol^{-1} for Spα, -20.1 deg·cm^2·dmol^{-1} for Spβ, and -24.9×10^3 deg·cm^2·dmol^{-1} for the Spα–Spβ complex (Fig. 2), corresponding to helical contents of 56% for Spα, 56% for Spβ, and 69% for the complex. Thus, the helical content increased ~13% in the complex at pH 6.5 and 20°C (NMR sample conditions), similar to the observations at pH 7.4 and 25°C (Mehboob et al. 2001).

Molecular weight, hydrodynamic radius, and molecular shape of complex

The weight-average molar mass (M_w) of Spα was 18.1 kDa (Fig. 3, dotted line), as determined by small-angle laser light-scattering measurements. For mixtures of Spα and Spβ (molar excess), the major peak (>70%) (Fig. 3, solid line) corresponded to a M_w of 42.5 kDa, a value very similar to the expected molecular mass for the Spα–Spβ complex (40.7 kDa for a total of 342 amino acid residues from Spα and Spβ, plus two residues remaining from thrombin cleavage for each protein). A small peak (~20% peak intensity) at 24.5 kDa was from excess Spβ in the sample. Prior to the major peak, the two small peaks at 1.4 MDa and 145 kDa (with <10% peak intensities) were assumed to be from oligomeric forms of the complex. These results showed that ~88% of the complex was monomeric at a concentration of ~0.3 mM. We also found that the M_w for SpαII was 17.8 kDa.

We obtained the hydrodynamic radius (R_H), the radius of a hard sphere that diffuses at the same rate as the protein, from dynamic light-scattering measurements for Spα, SpαII, and the Spα–Spβ complex. R_H is affected by the M_w, shape, and hydration of the protein. The R_H was 2.6 nm for Spα alone, 3.0 nm for SpαII, and 3.7 nm for the complex. The R_H value for the complex was larger than that of BSA (3.2 nm). It is interesting to note that the radius of gyration from small-angle X-ray scattering

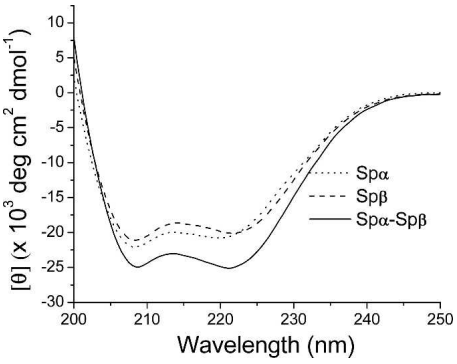

Figure 2. CD spectra of Spα (10 μM), Spβ (10 μM), and a mixture of Spα (5 μM) and Spβ (5 μM) in PBS, pH 6.5, at 20°C. Ellipticity (θ, mdeg) values from raw CD spectra were converted to mean residue ellipticity ([θ], deg·cm^2 · dmol^{-1}) values.

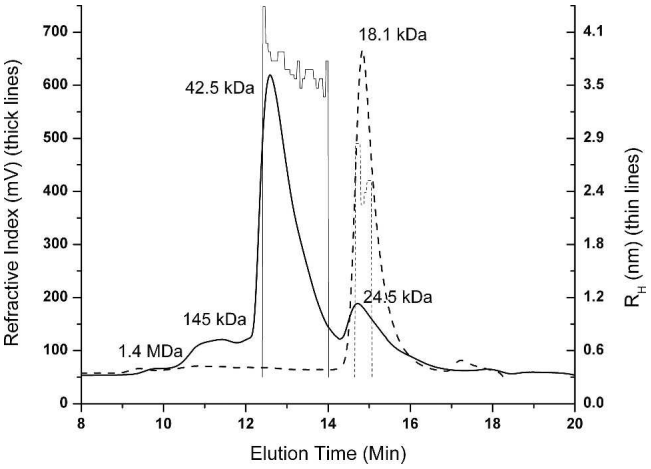

Figure 3. Chromatograms of Spα alone (thick dotted line) and of the Spα–Spβ complex (thick solid line). In both samples, the concentration for Spα was 0.3 mM. In the complex, the concentration for Spβ was 0.39 mM. A sample (100 μL) was injected onto a YMC Diol-200 (8.0 × 300 mm) column and eluted with PBS, pH 6.5, at a rate of 0.7 mL/min. Mass values from amino acid sequences are 18.6 kDa for Spα, 22.1 kDa for Spβ, and 40.7 kDa for the complex. Measured M_w values are 18.1 kDa for Spα alone and 42.5 kDa for the complex. The value for residual Spβ is 24.5 kDa. The two peaks with M_w of ~1.4 mDa and 145 kDa are likely to be oligomers of the complex. R_H tracings of Spα alone (thin dotted line) and of the complex (thin solid line) are also shown.

measurements was 2.45 nm for Spα and 2.95 nm for SpαII, with a R_g ratio ($R_g^{Spα}/R_g^{SpαII}$) of 0.83 (Mehboob et al. 2003), where R_g is the mass-weighted mean-square distance from the center of mass to every atom in the protein. The R_H ratio ($R_H^{Spα}/R_H^{SpαII}$) was 0.87.

We modeled Spα, SpαII, and the complex as prolate ellipsoids, each with a major axis *a* and a minor axis *b*. An anisotropic model (prolate ellipsoid) has been shown to fit the data significantly better than an isotropic model (Mackay et al. 1996). To calculate the Perrin shape parameter for the complex (F^{cx}), we used the shape information determined by small-angle X-ray scattering measurements for Spα and SpαII (Mehboob et al. 2003) to estimate $(a/b)_{Spα}$ as 2.3 and $(a/b)_{SpαII}$ as 3.2, where *F* is the ratio of the translational frictional coefficient of an ellipsoid (*f*) to that of a sphere with equal volume (f_{sph}) (Cantor and Schimmel 1987). The calculated value for $f^{Spα}/f^{SpαII}$ was 0.95, and the experimentally determined *k* was 0.92 (see Materials and Methods). With these values, F^{cx} was calculated to be 1.23, which corresponds to an *a*/*b* ratio of 4.7, indicating a highly asymmetric shape. It should be noted that SpαII was used here as a reference system for the ratio calculation simply because its shape was known and its sequence is similar to that of SpαI. Other proteins with known shape may also be used.

The translational self-diffusion coefficient (*D*) from pulsed-field gradient spin echo NMR experiments is often used to assess the oligomeric status and the shape of molecules to be studied by NMR for structural determination (Altieri et al. 1995) and was previously measured for free Spα (Park et al. 2000). Figure 4A shows that *D* for Spα alone was 0.96 ± 0.04 × 10^{-10} m^2/sec, which agreed well with previous measurements on Spα (Park et al. 1999, 2000). The *D* for the complex was 0.53 ± 0.04 ×10^{-10} m^2/sec. Since the diffusion coefficient and mass are related (Tanahatoe and Kuil 1997), our value of 0.53 × 10^{-10} m^2/s for the complex corresponded to a

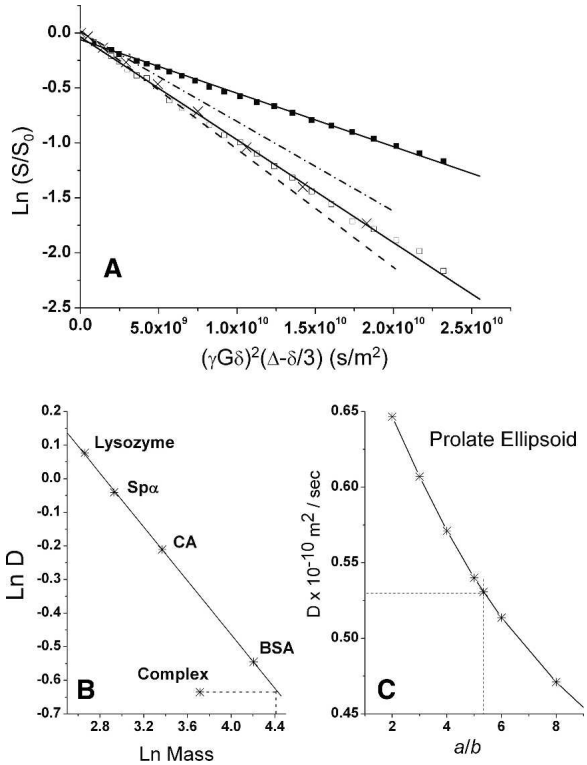

Figure 4. (*A*) Translational diffusion coefficient measurement using PFG-NMR, at 800 MHz, for Spα alone (0.20 mM; open squares) and the complex (1:1 molar ratio, each at 0.20 mM; solid squares) in PBS at pH 6.5 and 20°C, with S/S_o as normalized signal intensity, γ as proton gyromagnetic ratio, *G* as field gradient strength, δ as gradient pulse duration, and Δ as diffusion delay. The diffusion coefficients were calculated from the negative of the slopes using the equation $\ln(S/S_o) = -D(\gamma G\delta)^2(\Delta-\delta/3)$. Published results for Spα (Park et al. 2000) are shown as × symbols, with lysozyme as a dashed line and carbonic anhydrase as a dotted–dashed line. The coefficient value for Spα was 0.96 × 10^{-10} m^2/s, and that for the Spα–Spβ complex was 0.53 × 10^{-10} m^2/s. (*B*) Translational diffusion coefficient value for the complex, when compared with other globular proteins, corresponded to a protein of ~86 kDa. (*C*) An axial ratio *a*/*b* of 5.3 was obtained from the plot of *a*/*b* values of prolate ellipsoid versus translational diffusion coefficient values. *D* values for a prolate ellipsoid with different axial ratio values, and thus different Perrin shape parameter *F*, were calculated for a protein with M_w of 42.5 kDa, using the following quation: $D/D^{BSA} = [F/(M_w)^{1/3}]/[F^{BSA}/(M_w^{BSA})^{1/3}]$, with D^{BSA} = 0.53 × 10^{-10} m^2/s, F^{BSA} = 1, and M_w^{BSA} = 67 kDa (Gribbon and Hardingham 1998).

globular molecule with a mass of ~86 kDa (Fig. 4B). Published values (Gribbon and Hardingham 1998) of 1.08×10^{-10} m^2/s for lysozyme (14.3 kDa), 0.81×10^{-10} m^2/s for carbonic anhydrase (29 kDa), and 0.58×10^{-10} m^2/s for bovine serum albumin (67 kDa) were used for Figure 4B. The coefficients calculated for a prolate ellipsoid with various values for the Perrin shape parameter F, using BSA ($a/b = 1$) as a reference, showed that the measured D for the complex corresponded to an axial ratio of 5.3 (Fig. 4C). This value agreed well with the value of 4.7 derived from the R_H values measured by dynamic light-scattering methods.

Thus, our results from static and dynamic light-scattering measurements, as well as from pulsed-field gradient spin echo NMR measurements, showed that the Spα–Spβ complex was in monomeric form at a concentration as high as 0.3 mM and was highly asymmetric, corresponding to a prolate ellipsoid with an axial ratio of ~5.

Dynamics and conformation of Spα in Spα–Spβ complex

In our previous NMR studies at 600 MHz, 149 residues out of 153 (156 less the P5, P15, and P84 residues) of Spα residues were assigned (Park et al. 1999, 2000, 2003). The current HSQC of free ^{15}N-Spα (Fig. 5A) and the TROSY of ^{2}H,^{15}N-Spα (Fig. 5C) at 900 MHz were essentially identical to those obtained at 600 MHz, making signal identification for this study relatively straightforward. In free Spα samples, the TROSY signal intensities/amplitudes (Fig. 6, open symbols) for those residues previously identified as being in unstructured regions that sandwich helices (residues 1–20, 46–52, 82–87, 119–122, and 154–156) were relatively high, while the intensities for those in helical regions, consisting of Helix C′, the partial domain (residues 21–45), Helix A_1 (residues 53–81), Helix B_1 (residues 88–118) and Helix C_1 (residues 123–153) in the first structural domain (Park et al. 2003), were relatively low.

Upon addition of 1.4 molar excess of unlabeled Spβ to Spα, much-simplified HSQC (Fig. 5B) and TROSY spectra (Fig. 5D) were obtained. The number of scans was 20 times more than those for samples of free Spα in HSQC and four times more in TROSY (see Materials and Methods). The TROSY signal intensities for residues 1–14 remained relatively high (Fig. 6, closed symbols), while the intensities for the residues in the two disordered loop regions within the helical bundle structural domain were relatively lower. However, even with four times

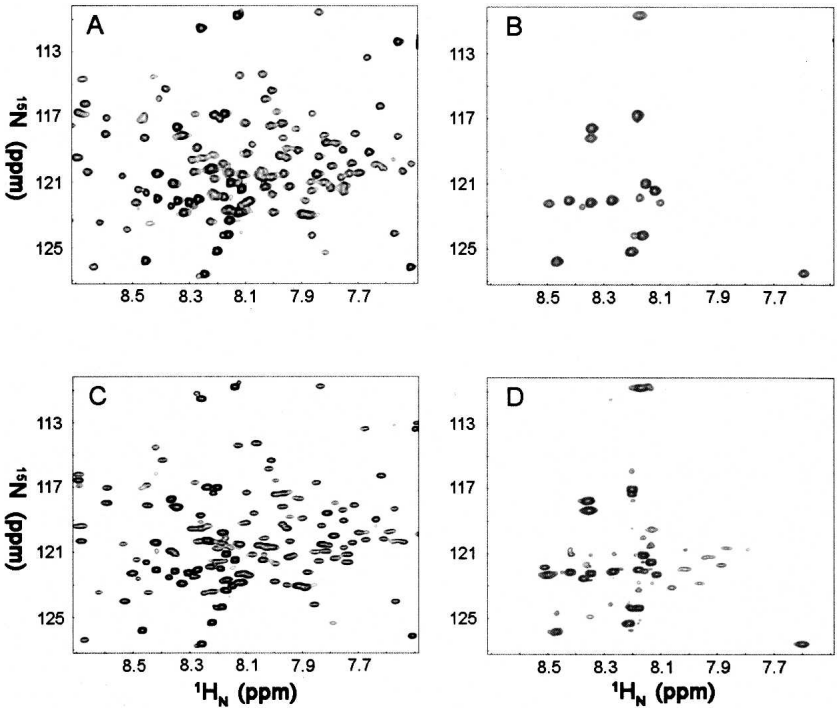

Figure 5. HSQC spectra of ^{15}N-labeled Spα alone (0.30 mM, 8 scans) (*A*) and in the presence of molar excess, unlabeled Spβ (160 scans) (*B*). TROSY-HSQC of ^{15}N,^{2}H-labeled Spα alone (0.30 mM, 16 scans) (*C*), and Spα (0.30 mM) in the presence of molar excess unlabeled Spβ (64 scans) (*D*). All samples were in PBS, pH 6.5. NMR spectra were taken at 20°C on a Bruker 900-MHz spectrometer. A total of 1536 × 256 complex points were acquired with sweep widths of 12,626 × 3283 Hz in the direct and indirect dimensions, respectively.

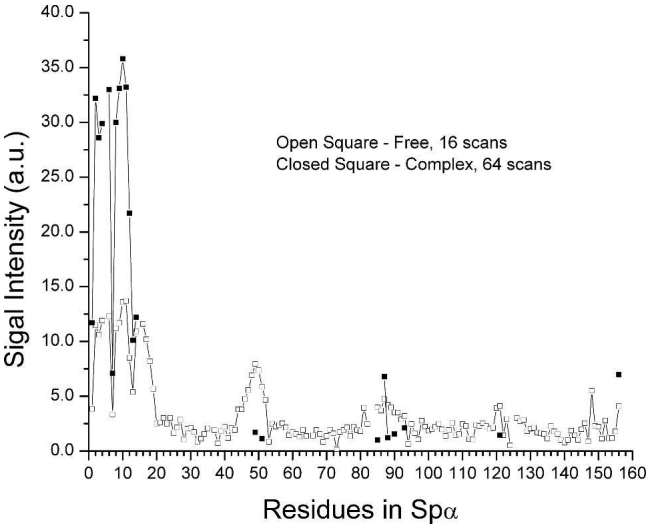

Figure 6. TROSY-HSQC signal intensity of the Spα residues without (open symbols, 16 scans) and with Spβ (closed symbols, 64 scans). See Figure 5C and D, for spectra and sample conditions.

more scans, we were unable to detect signals for residues in helices C′, A_1, B_1, and C_1. Interestingly, the signal intensities for residues 16–20 and 46–52 were very low or not observed. In free Spα, their intensities were relatively high and were similar to those of residues 1–14, as these residues are in the unstructured regions.

A more systematic monitoring of the signal intensity reduction of Spα was obtained by titrating ^{15}N-Spα with unlabeled Spβ. HSQC spectra of the titration showed that the normalized signal intensities of residues 1–12 in the unstructured region remained about the same throughout the titration (Fig. 7A, top). In addition, the intensities of residues 83 and 87 in the loop region (residues 82–87) remained about the same in these samples, whereas the intensities of residues 85 and 86 decreased steadily upon addition of Spβ. Residue 84 is a proline. The signals for residues in short loops (residues 119–122 between Helix B_1 and Helix C_1 and 154–155 at the end of the structural domain) decreased similarly to those of residues 85 and 86.

The intensity decreases for residues 13 (8.32/117.50 ppm), 14 (8.13/110.24 ppm), and 156 (7.51/125.70 ppm) were also quite similar to those for residues 85 and 86. However, these three residues also appeared as new peaks upon addition of Spβ, with the peak positions shifted very slightly from the original peaks (Fig. 8). The total signal intensities of these three residues decreased less rapidly than the decrease of free Spα species in solution (Fig. 7A, bottom).

Signal intensity for the remaining residues (residues 16–82 and 88–155) decreased rather uniformly (Fig. 7B) and correlated *quantitatively* to the amounts of free Spα in the samples calculated from ITC data (Fig. 1). It is interesting to note that a K_d value of ~1 μM was obtained from the HSQC titration results, in good agreement with that obtained by ITC measurements.

We observed no increase in the line widths of signals from residues in free Spα during the titration.

We also compared the HSQC spectra of SpαII to the spectra of its tightly associated SpαII-Spβ complex (the association affinity was 250-fold higher than that of Spα-Spβ complex). Similar to the Spα-Spβ complex, only a few SpαII peaks were detectable in the spectrum of the SpαII-Spβ complex when compared to the free SpαII spectrum (data not shown; at this time, we do not have residue assignments for SpαII.).

For the HSQC signal broadening in the complex, there are generally two intermediate timescale exchanges that could be induced by the binding: intramolecular exchange and intermolecular exchange (Lu et al. 2006). Intramolecular exchange can certainly induce generalized conformational changes of residues not directly involved in binding interactions through, for example, an allosteric mechanism (Lu et al. 2006). However, this mechanism does not apply to our system. If intramolecular exchange were the main mechanism of signal decay, then we would have to assume that there were similar ''degrees'' of exchange throughout the helical regions because their signal decay patterns are very uniform among the residues.

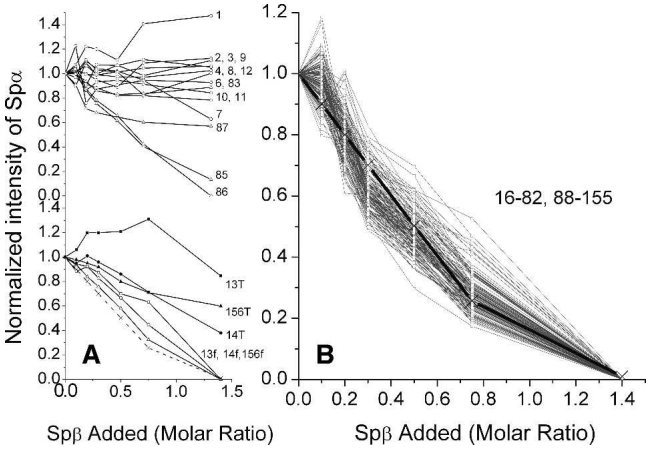

Figure 7. Normalized HSQC intensity (nNH_{ij}; see Materials and Methods) of all detectable signals for residues 1–156 of Spα in mixtures with Spβ/Spα molar ratios of 0.1, 0.2, 0.3, 0.5, 0.75, and 1.4. Calculated amounts of free Spα in each mixture, shown as a dotted line in panel *A* and as a thick black line in panel *B*, are from Figure 1 *inset*. Signals for residues with no detectable chemical shift changes upon addition of Spβ are shown as open symbols in the *top* of panel *A* for residues 1–12 except P5 (symbol: ○), and residues 83–87 except P84 (symbol: △) and in panel *B* for residues 16–82 and 88–155. Those with slight chemical shift changes upon addition of Spβ (residues 13, 14, and 156) (*bottom* of panel *A*) are shown with open symbols for signals at chemical shifts of free state (13f, 14f, and 156f) and with closed symbols for total signals (13T, 14T, and 156T).

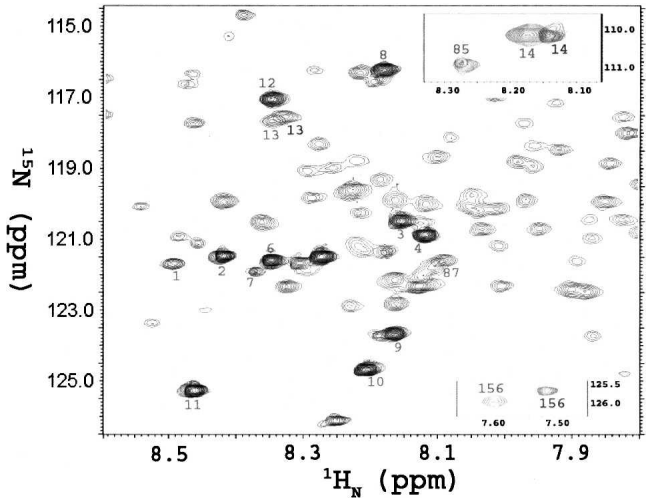

Figure 8. Overlapping HSQC spectra for Spα (light) and Spα–Spβ complex (dark, with peaks numbered 1–4, 6–14, 83, 85, 87, and 156) at 900 MHz. The spectra of ^{15}N-Spα (0.40 mM) in PBS at pH 6.5, with 95% H_2O and 5% $^{2}H_2O$, were accumulated for eight scans (20 min). Spectra of ^{15}N-Spα, or SpαII, with excess unlabeled Spβ (0.56 mM to give Spβ/Spα molar ratios of 1.4) were accumulated for 160 scans (6.7 h). Peaks 13, 14, and 156 in complex were shifted slightly. Most of the signals observed in samples of Spα alone were not detected in samples of the Spα–Spβ complex.

If we assume residues in the unstructured region underwent structural transition, then the equivalent degree of transitions for helical residues, or helical-to-unstructured transitions, should be present. However, this is not consistent with our CD results that showed increased helicity upon binding, and it would also contradict the general consensus that the triple-helical bundle is retained in the Spα–Spβ complex. This analysis suggests that intramolecular exchange is an unlikely mechanism.

The 1 μM binding affinity implies that the intermolecular interaction is in slow exchange, assuming diffusion-limited association, and suggests that the intermolecular intermediate timescale exchange is not responsible for HSQC line broadening. This is consistent with the fact that the SpαII–Spβ complex, which exhibits a 4 nM dissociation constant further favoring the slow exchange region, exhibits similar line-broadening patterns. Thus, we believe that the most likely mechanism for the HSQC line broadening is due to asymmetric rigid body rotation of the complex.

Results from phase-modulated CLEAN chemical exchange experiments for free ^{15}N-Spα samples showed the backbone NH solute–solvent exchange signals from residues 1–18 (excluding P5 and P15), 45–52, 81, 83–96 (excluding P84 and except 91), and 121–122 (Fig. 9). These are residues in the unstructured regions with observable solute–solvent exchange signals. For Spα in complex, residues 1–14 showed CLEANEX-PM signals (Fig. 9), indicating that, in the complex, these residues remained unstructured and without backbone hydrogen bonding, whereas residues 16–20 and 46–52 were no longer similar to the residues 1–14 but were more like those in helical regions.

Discussion

We previously determined the NMR solution structure of a recombinant protein derived from the sequence of the first 156 residues of human erythrocyte α-spectrin (SpαI-1–156, or Spα) (Fig 10). This protein consists of the region responsible for α-spectrin associating with its partner, β-spectrin, to form functional tetramers and exhibits an association affinity with β-spectrin similar to that of the intact full-length α-spectrin (Mehboob et al. 2003). The NMR structure shows a total of 40 residues (residues 1–20, 46–52, 82–87, 119–122, and 154–156) in unstructured regions and a total of 116 residues in helices, in between the unstructured regions, with residues 21–45 forming the first helix (Helix C′, often called the partial domain of α-spectrin), and residues 53–81, 88–118, and 123–153 forming the three helices of the first triple-helical bundle structural domain (helices A_1, B_1, and C_1) (Park et al. 2003), with a helical content of ~74%. Thus, Spα is a highly helical protein molecule. One of the most unexpected and interesting features in this protein is the independent mobility of the partial domain Helix C′ relative to the first structural domain (the triple-helical bundle), due to an unstructured, and thus a very flexible junction region between Helix C′ and the first structural

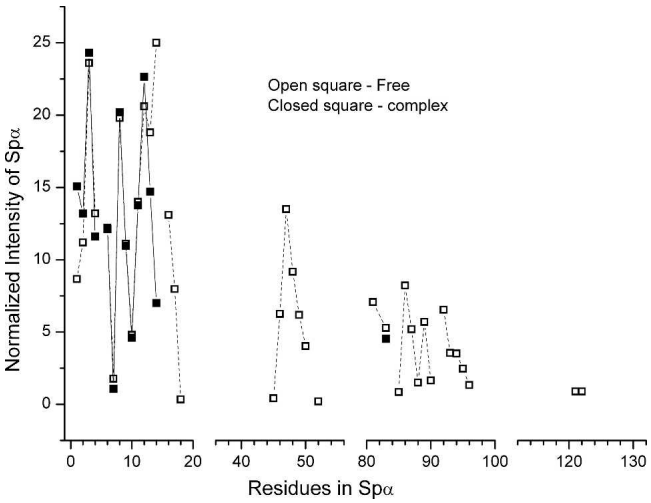

Figure 9. Normalized CLEANEX-PM signal intensities of ^{15}N-Spα (0.25 mM) and of Spα–Spβ mixtures (1:1.4 molar ratio). The spin-locking field was 5.0 kHz. Three different mixing times (75, 100, and 150 ms) were used, and no significant differences were observed. Accumulation time was 64 scans for Spα and 160 scans for Spα–Spβ mixture samples.

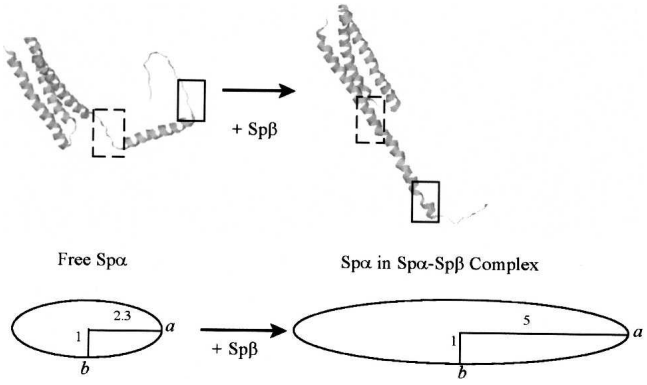

Figure 10. NMR structure of Spα (Protein Data Bank: 1OWA) (*left*), showing the regions prior to (dashed-line square) and following (solid-line square) Helix C′ in an unstructured conformation, and a model structure of Spα in Spα–Spβ complex (*right*), showing the regions prior to (dashed-line square) and following (solid-line square) Helix C′ in a helical conformation. A prolate ellipsoid model, with a major (long) axis of ~5 and a minor (short) axis of 1, was used to represent a rigid and asymmetric shape of the complex.

domain. The flexibility of this junction region may be an important characteristic of erythroid spectrin, since it may contribute to the relatively low binding affinity with Spβ in erythroid spectrin (μM range), as compared to that of non-erythroid spectrin (nM range) (Mehboob et al. 2005).

Our CD studies have shown an increase in helical content in the Spα–Spβ complex at pH 7.4 (Mehboob et al. 2001), although the details of the conformational change(s) are not known. In this study, CD data at pH 6.5 showed an increase of ~10% in the helical content in the complex, similar to that observed at pH 7.4. The helicity values from CD studies are obtained from the commonly used value of $[\theta]_{222}$ at −36,000 deg·cm^2·dmol^{-1} as 100% helicity (see Materials and Methods). For Spα alone, the helical content from CD measurements was 56%, whereas the more accurate value from NMR is 74%, yielding a conversion factor of 74/56. The helical content of the complex, from CD measurements, increased to 69%. If it is assumed that the helices in the complex are similar to those in free Spα, then the CD helical content of 69% would correspond to an NMR content of ~91%, or ~30 residues in the complex being unstructured. Since Spα alone has 40 residues in a non-helical conformation, it is possible that all the changes occurred in Spα. Of course, it is equally possible that changes occurred in both Spα and Spβ. Since no structural information for Spβ is available at this time, it is not possible to speculate how many of these residues are from Spα and how many from Spβ. However, our results show that at least 12 residues from Spα are involved in disordered-to-helical conformational changes.

Hydrodynamic studies indicated that the complex was monomeric and exhibited a highly asymmetric shape at a concentration of 0.30 mM in PBS at pH 6.5. When modeled with a prolate ellipsoid, its major axis would be about five times longer than the minor axis (Fig. 10).

In principle, since we already have the NMR assignments for the Spα residues, it should be relatively simple to determine specific residues/regions undergoing conformational change(s) upon binding Spα by monitoring Spα with TROSY-HSQC methods in Spα–Spβ complex. TROSY selects only one of the four transitions—the one that is insensitive to Brownian motion in a high magnetic field. The optimal frequency for the TROSY effect is calculated to be near 1000 MHz (Pervushin et al. 1997). Thus, our 900-MHz spectra should be near ideal for structural studies of proteins with rather high M_w. However, the solubilities of Spα, Spβ, and Spα–Spβ complex were relatively low for NMR measurements of such asymmetric molecules. To avoid aggregation, we used samples with concentrations at or below 0.30 mM. Many signals were not detectable in the complex at these concentrations, even with 64 scans (four times more than for samples with Spα alone at the same concentration). Additional data accumulation led to aggregate formation in samples due to the long observation time. However, despite the low solubility and asymmetric shape of the complex molecules, we clearly observed dramatic spectral changes for 12 residues in Spα that provide useful information related to conformation changes in Spα upon binding Spβ.

Our results showed that, upon complex formation, seven residues prior to Helix C′ and five following Helix C′ in the unstructured region of free Spα exhibited NMR properties different from those of other unstructured residues in the complex. Instead, their NMR properties were more similar to those previously identified as being in a helical conformation. Therefore these are likely to be residues that underwent conformational changes upon binding to Spβ. A particularly interesting change was observed for residues 46–52, the junction region between Helix C′, and the structural domain. An unstructured to helical conformational change in the junction region would restrict the motion of Helix C′, making the complex more rigid and highly asymmetric.

One may argue that, in the complex, the five residues at positions 16–20 (KVLET) and seven residues at positions 46–52 (GQKLEDS) flanking both ends of Helix C′ (Fig. 10). exhibit restricted motions simply due to side-chain interactions with those in Spβ rather than being due to helix formation. There are two positively charged side chains (K16 and K48) and three negatively charged side chains (E19, E50, and D51) in these 12 residues that may interact with the side chains in Spβ, as shown in our published working model of Spβ (Mehboob et al. 2001). However, it is not clear why the side chains of the first 15 residues (MWQFPKETVVESSGP), also consisting of

positively and negatively charged side chains, would not also interact with the side chains of Spβ to become ''rigid'' residues in the complex, thus producing signals broadened beyond detection. Thus, the possibility that only residues 16–20, and not residues 1–12, exhibit restricted motions simply due to side-chain interactions with Spβ appears low.

Based on the published helix-propensity scale (Pace and Scholtz 1998), we obtained the free energy required to form a helical conformation for residues 16–20 as 8.95 kJ/mol (1.79 kJ/mol per residue) and for residues 46–52 as 14.43 kJ/mol (2.06 kJ/mol per residue). However, based on the same scale, it would take 51.98 kJ/mol (3.47 kJ/mol per residue) for residues 1–15 to form a helical conformation. Thus, it is energetically more likely for residues 16–20 and 46–52 to convert to a helical structure than for residues 1–15 to do so.

The possibility that the unstructured regions may convert to structured/helical regions (Fig. 10) is intriguing. Numerous examples have shown disorder–order transitions in proteins. For example, the CREB kinase-inducible activation domain is unstructured in solution and undergoes an α-helix folding transition on binding to its coactivator CBP (Hua et al. 1998), and the unstructured 15-amino acid S-peptide forms a helix when it binds to S-protein (Goldberg and Baldwin 1999). Generally, the potential advantages for disorder–order transitions in proteins are numerous (Uversky 2002). For the Spα and Spβ system, a disorder–order transition may provide a modulation in the thermodynamics of Spα–Spβ association. The nonerythroid Spα (SpαII) associates with Spβ with much higher affinity, with a K_d of ~0.004 μM, than the micromolar K_d of Spα and Spβ, or a $\Delta G°$ difference of ~13.7 kJ/mol. This free-energy difference is similar to the free-energy difference to form α-helical segments in these two isoforms. There are only two amino acid differences in these two regions (prior to and following Helix C′), with P15 in Spα and V6 for SpαII, and 46G for Spα and 37R for SpαII (note: Sequence numbering differs by 9 between Spα and SpαII). Both proline and glycine exhibit low helix propensities (Pace and Scholtz 1998), and the $\Delta G°$ for converting P and G from unstructured to helical is 4.16 kcal/mol (using 3.16 kcal/mol for P and 1.00 kcal/mol for G from published work of Pace and Scholtz [1998]), whereas the $\Delta G°$ for converting V and R from unstructured to helical is 0.82 kcal/mol (using 0.61 kcal/mol for V and 0.21 kcal/mol for R). Thus the $\Delta\Delta G°$ is 3.34 kcal/mol, or 13.96 kJ/mol. It is intriguing to speculate that the lower affinity in Spα–Spβ association, when compared with SpαII–Spβ, is due to the free energy needed to convert the previously nonhelical segments to helical segments in Spα, and that this free energy is not necessary in SpαII due to its sequence difference that gives it a higher helical propensity.

It is also interesting to note that, although residues 46–52 are in the unstructured region in free Spα, and were not generally expected to be involved in the binding of its β-partner, mutations at some of these positions (such as G46V, K48R, and L49F) are hematologically critical (Gallagher and Forget 1996). Our results suggest that, for mutant L49F (with $\Delta G°$ for converting from unstructured to helical being 0.21 kcal/mol for L and 0.54 kcal/mol for F), it is not energetically favorable to convert the region of residues 46–52 from disordered to helical conformation, and thus it exhibits a decreased αβ association affinity to give low levels of tetramers. Other mechanisms would apply to G46V and K48R mutants since these mutations make the disordered-to-helical conformation changes easier, based on helical propensity.

In summary, this study showed that Helix C′ in Spα no longer moved independently in the Spα–Spβ complex due to conformational changes of residues flanking the two ends of Helix C′, that converted them from an unstructured to a helical conformation upon association with β-spectrin. The relatively low affinity in erythroid α- and β-spectrin association, as compared to nonerythroid spectrin association, is likely due, at least in part, to the unstructured regions flanking the partial domain helix in α-spectrin. Our studies also provide a mechanism for explaining why patients with L49F mutation have low concentrations of spectrin tetramers.

Materials and Methods

Spectrin recombinant proteins

SpαI-1–156 (Spα), ^{15}N-labeled Spα (^{15}N-Spα), ^{15}N- and ^{2}H-labeled Spα (^{15}N,^{2}H-Spα), and SpβI-1898–2083 (Spβ) were expressed and purified as before (Mehboob et al. 2001; Park et al. 2003). Individual proteins, in 5 mM phosphate buffer containing 150 mM NaCl (PBS) at pH 7.4 (PBS7.4), were purified to at least 95% purity, as indicated by SDS gel electrophoresis results. Protein masses from a high-resolution/high mass accuracy LTQ-FT mass spectrometer showed about 99% ^{15}N labeling in ^{15}N-Spα samples and 70% ^{2}H labeling of CH groups in ^{15}N,^{2}H-Spα samples.

A new protein (SpαII) consisting of the first 147 residues of brain α-spectrin, derived from SpαII-1–149 (Mehboob et al. 2003), was also labeled with ^{15}N for hydrodynamic and NMR measurements.

It is important to note that all samples were prepared in PBS at pH 6.5, which was more desirable for NMR measurements than pH 7.4. Due to the lower solubility of Spβ at pH 6.5, and the lower solubility of Spβ than of the Spα–Spβ complex, the complex samples at ~0.3 mM were prepared by mixing Spα and Spβ at lower concentrations (Spα at ~0.02 mM and Spβ at different molar ratios) in PBS at pH 7.4, then dialyzing overnight in PBS at pH 6.5, and concentrating to higher, desirable concentrations. No precipitation was observed in samples during or after experimental measurements. All samples were also checked for degradation by SDS gel electrophoresis before and after experiments and for oligomerization by light-scattering

methods (see below). Only data from samples with identical before-and-after gel patterns (no degradation) and without any oligomers after experiments were used.

Isothermal titration calorimetry (ITC)

ITC measurements were performed with samples in PBS at pH 6.5 (PBS6.5) at 20°C using a VP-ITC unit (MicroCal) as described elsewhere (Mehboob et al. 2003). Multiple (usually 25–30) injections of 8 μL of Spα (0.31 mM) were introduced into the sample cell containing Spβ (1.45 mL at 0.014 mM). For SpαII and Spβ titration, the concentration for SpαII was 0.025 mM and that for Spβ was 0.0023 mM. Data were analyzed with the Origin software provided by MicroCal, using a single binding site model to give values of K_d, n, $\Delta H°$, $\Delta S°$, and $\Delta G°$.

Circular dichroism (CD)

Samples of Spα (0.01 mM), Spβ (0.01 mM), and a mixture of Spα (0.005 mM) and Spβ (0.005 mM) in PBS at pH 6.5 were used for CD measurements at 20°C, with a JASCO 810 CD spectrometer. Ellipticity (θ, mdeg) values from CD spectra were converted to mean residue ellipticity ([θ], $\text{deg}\cdot\text{cm}^2\cdot\text{dmol}^{-1}$) values. Helicities were then calculated from the [θ] values at 222 nm ($[\theta]_{222}$), using a value of −36,000 $\text{deg}\cdot\text{cm}^2\cdot\text{dmol}^{-1}$ as 100% helicity (Mehboob et al. 2001). The $[\theta]_{222}/[\theta]_{208}$ ratios for all three samples were also obtained to determine the presence or absence of paired helices (Mehboob et al. 2001).

Static and dynamic light scattering

A setup for both static and dynamic light-scattering measurements (PD2000 system, Precision Detectors, Inc.) with a size-exclusion column (YMC Diol-200) was used to study the molecular size and shape of Spα at 0.30 mM, alone, and with a molar excess of Spβ. Light intensity scattered at 90° and refractive index signals of each sample (100 μL) were measured, and the weight-average molar mass (M_w) values were calculated. The hydrodynamics' radii (R_H) of Spα and of the complex were obtained, with the instrument operating in the flow mode and using the dynamic light-scattering photon detector, from the decay time of the autocorrelation function of the scattered light.

With the R_H values of Spα, SpαII, and the complex, and by modeling these asymmetric proteins as prolate ellipsoids, we calculated the Perrin shape parameter (F), and thus the values for the major (a) and minor (b) axes, of the complex (using Equations 10–19a in Cantor and Schimmel 1987). The Perrin shape parameter is the ratio of the frictional coefficient of an ellipsoid (f) to that of a sphere with equal volume (f_{sph}) (Cantor and Schimmel 1987), and f is proportional to R_H. Hydrodynamic properties depend on hydration, shape, temperature, viscosity of the solution, etc. However, assuming these factors were the same for the systems 1 and 2, then $f^1/f^2 = kR_H{}^1/R_H{}^2$, where k is 1 if all experimental uncertainties for related parameters were the same; otherwise, the k value would be determined experimentally. From the published shape of Spα and SpαII, as determined by small-angle X-ray scattering measurements (Mehboob et al. 2003), we estimated $(a/b)_{Spα}$ as 2.3 (Fig. 10), which gave a value of $F^{Spα}$ as 1.06 and $(a/b)_{SpαII}$ as 3.2, which gave a value of $F^{SpαII}$ as 1.13. $F^{Spα}/F^{SpαII} = 1.06/1.13 = 0.94$. With this value, we calculated $f^{Spα}/f^{SpαII}$, since $f^{Spα}/f^{SpαII} = (F^{Spα}/F^{SpαII}) \times (f_{sph}{}^{Spα}/f_{sph}{}^{SpαII}) = (F^{Spα}/F^{SpαII}) \times (M_w{}^{Spα}/M_w{}^{SpαII})^{1/3}$. Finally, for the complex, $F^{cx} = R_H{}^{cx}/R_H{}^{Spα} \times 1/k \times F^{Spα} \times [(M_w{}^{cx})/M_w{}^{Spα})]^{-1/3}$.

NMR samples

NMR samples were prepared in PBS at pH 6.5, with 95% H_2O and 5% D_2O (Park et al. 1999, 2000, 2002, 2003). NMR samples containing labeled or unlabeled Spα and Spβ were mixed with Spα (~0.02 mM) and Spβ (at different molar ratios) in PBS at pH 7.4, then dialyzed overnight in PBS at pH 6.5, and concentrated to higher, desirable concentrations. As indicated above, only data from samples with identical before-and-after gel patterns (no degradation) and without any oligomers after NMR runs were used.

Translational self-diffusion coefficient measurements

Samples of Spα (0.25 mM), alone or with equimolar Spβ, were used. The spectra were obtained with a Bruker 800-MHz instrument (AVANCE) at 20°C as before (Park et al. 2000) to give the translational self-diffusion coefficients of Spα, with and without Spβ. The value for Spα only was compared with our published value (0.96×10^{-10} m^2/s) (Park et al. 2000).

Theoretical translational diffusion coefficients for a prolate ellipsoid with a particular M_w value but with several different axial ratios were calculated, using the equation $D/D_{BSA} = [F/(M_w)^{1/3}]/[F_{BSA}/(M_{w\text{-}BSA})^{1/3}]$ where D is the diffusion coefficient and F is the Perrin shape parameter for ellipsoids (Cantor and Schimmel 1987).

HSQC, TROSY-HSQC, and CLEANEX-PM experiments

All spectra were obtained on a Bruker 900-MHz spectrometer (AVANCE), equipped with an ATM (automatic tuning and matching) triple-resonance probe.

$^1H,^{15}N$ Transverse relaxation-optimized spectroscopy (TROSY-HSQC, or simply TROSY) experiments at 20°C were carried out on $^2H,^{15}N$-Spα (0.30 mM), alone or with a 1.4 molar excess of unlabeled Spβ. TROSY spectra were accumulated with 16 scans (1.8 h) for Spα and 64 scans for the complex. A total of 1536 × 256 complex points were acquired with sweep widths of 12,626 × 3283 Hz in the direct and indirect dimensions, respectively. All spectra were collected with a recycle delay of 1 s. $^1H,^{15}N$-HSQC experiments at 20°C were carried out as before (Park et al. 1999, 2000, 2002, 2003) on samples 1–7, with sample 1 being ^{15}N-Spα alone (Spβ/Spα molar ratio of 0) and samples 2–7 being ^{15}N-Spα titrated with unlabeled Spβ, with molar ratios of 0.1, 0.2, 0.3, 0.5, 0.75, and 1.4, respectively. The final concentrations of ^{15}N-Spα in all samples were 0.30 mM. The accumulation time for HSQC spectra ranged from 20 min (eight scans) for sample 1 to 6.7 h (160 scans) for sample 7.

Phase-modulated CLEAN chemical exchange (CLEANEX-PM) (Hwang et al. 1998) experiments, with ^{15}N-Spα at 0.25 mM, were carried out on samples 1 (Spα alone) and 7 (Spα with 1.4 molar excess Spβ). Three different mixing times (75, 100, and 150 ms) were used; however, no systematic differences were observed. The spin-locking field was 5.0 kHz. The accumulation time for CLEANEX-PM was ~3 h (64 scans) for sample 1 and ~7.5 h (160 scans) for sample 7.

All raw data were processed by NMRPipe (Delaglio et al. 1995) and further analyzed with either NMRDraw of NMRPipe or NMRView (Johnson and Blevins 1994). Assignments of ^{15}N-Spα resonances obtained previously (Park et al. 2003) were used. The raw HSQC signal intensities of each residue in each of the 7 samples (NH_{ij}, where i is the residue number, 1–156, and j is the sample number, 1–7) were obtained. Since instrumental factors such as shimming and tuning may affect NH_{ij} values, the NH_{ij} values of sample j were normalized. We first obtained an average value of the intensities of residues 1–10 in sample j [$A_j = (1/10)\sum NH_{ij}$, with i = 1–10]. Since the intensities of residues 1–10 remained similar for all seven samples (see discussion below), the average value of these intensities in a sample was used as a reference value for the intensities of other residues in that sample. So for sample j, the NH_{ij} values were first "formatted" with A_j to give $fNH_{ij} = NH_{ij}/A_j$, with i = 1–156, and then normalized to give $nNH_{ij} = fNH_{ij}/fNH_{i1}$ for j = 2–7, where fNH_{i1} were the values of sample 1.

The intensity values obtained in CLEANEX-PM experiments were simply normalized with the number of scans, 64 scans for Spα and 160 scans for the Spα–Spβ complex, for easy comparison.

Acknowledgments

We thank Drs. Yoshitaka Ishii and Michael E. Johnson of the University of Illinois at Chicago for discussions on magnetic relaxation properties of asymmetric molecules. We thank Dr. B.G. Forget of Yale University School of Medicine for the cDNA of erythroid spectrin and Dr. R.T. Moon of the University of Washington School of Medicine for the cDNA of non-erythroid α-spectrin. This work was supported in part by grants from the American Heart Association (0350617Z to L.W.-M.F.), the National Institutes of Health (GM68621to L.W.-M.F.), and an Inha University research grant (INHA-32729-01 to S.P.). The 800-MHz NMR instrument was funded by NSF through grant BIR0079604, and the 900-MHz NMR instrument by NIH through P41 GM68944. The high-resolution/high mass accuracy LTQ-FT mass spectrometer was supported by grants from the Searle Funds at the Chicago Community Trust to the Chicago Biomedical Consortium and the University of Illinois at Chicago Research Resources Center.

References

Altieri, A.S., Hinton, D.P., and Byrd, R.A. 1995. Association of biomolecular systems via pulsed field gradient NMR self-diffusion measurements. *J. Am. Chem. Soc.* **117:** 7566–7567.

Beck, K.A. 2005. Spectrins and the Golgi. *Biochim. Biophys. Acta* **1744:** 374–382.

Beck, K.A. and Nelson, W.J. 1998. A spectrin membrane skeleton of the Golgi complex. *Biochim. Biophys. Acta* **1404:** 153–160.

Begg, G.E., Morris, M.B., and Ralston, G.B. 1997. Comparison of the salt-dependent self-association of brain and erythroid spectrin. *Biochemistry* **36:** 6977–6985.

Begg, G.E., Harper, S.L., Morris, M.B., and Speicher, D.W. 2000. Initiation of spectrin dimerization involves complementary electrostatic interactions between paired triple-helical bundles. *J. Biol. Chem.* **275:** 3279–3287.

Bennett, V. and Baines, A.J. 2001. Spectrin and ankyrin-based pathways: Metazoan inventions for integrating cells into tissues. *Physiol. Rev.* **81:** 1353–1392.

Bignone, P.A. and Baines, A.J. 2003. Spectrin αII and βII isoforms interact with high affinity at the tetramerization site. *Biochem. J.* **374:** 613–624.

Broderick, M.J. and Winder, S.J. 2005. Spectrin, α-actinin and dystrophin. *Adv. Protein Chem.* **70:** 203–246.

Cantor, C.R. and Schimmel, P.R. 1987. *Biophysical chemistry,* part 2, pp. 560–564. Freeman, San Francisco, CA.

Delaglio, F., Grzesiek, S., Vuister, G.W., Zhu, G., Pfeifer, J., and Bax, A. 1995. NMRPipe: A multidimensional spectral processing system based on UNIX Pipes. *J. Biomol. NMR* **6:** 277–293.

Delaunay, J. and Dhermy, D. 1993. Mutations involving the spectrin heterodimer contact site: Clinical expression and alterations in specific function. *Sem. Hematology* **30:** 21–33.

DeSilva, T.M., Peng, K.C., Speicher, K.D., and Speicher, D.W. 1992. Analysis of human red cell spectrin tetramer (head-to-head) assembly using complementary univalent peptides. *Biochemistry* **31:** 10872–10878.

Gallagher, P.G. and Forget, B.G. 1996. Hematologically important mutations: Spectrin variants in hereditary elliptocytosis and hereditary pyropoikilocytosis. *Blood Cells Mol. Dis.* **22:** 254–258.

Gascard, P. and Mohandas, N. 2000. New insights into functions of erythroid proteins in nonerythroid cells. *Curr. Opin. Hematol.* **7:** 123–129.

Goldberg, J.M. and Baldwin, R.L. 1999. A specific transition state for S-peptide combining with folded S-protein and then refolding. *Proc. Natl. Acad. Sci.* **96:** 2019–2024.

Goodman, S.R. 1999. Discovery of nonerythroid spectrin to the demonstration of its key role in synaptic transmission. *Brain Res. Bull.* **50:** 345–346.

Goodman, S.R., Zagon, I.S., and Kulikowski, R.R. 1981. Identification of a spectrin-like protein in nonerythroid cells. *Proc. Natl. Acad. Sci.* **78:** 7570–7574.

Gribbon, P. and Hardingham, T.E. 1998. Macromolecular diffusion of biological polymers measured by confocal fluorescence recovery after photobleaching. *Biophys. J.* **75:** 1032–1039.

Grum, V.L., Li, D., MacDonald, R.I., and Mondragon, A. 1999. Structures of two repeats of spectrin suggest models of flexibility. *Cell* **98:** 523–535.

Harper, S.L., Begg, G.E., and Speicher, D.W. 2001. Role of terminal non-homologous domains in initiation of human red cell spectrin dimerization. *Biochemistry* **40:** 9935–9943.

Hua, Q., Jia, W., Bullock, B.P., Habener, J.F., and Weiss, M.A. 1998. Transcriptional activator–coactivator recognition: Nascent folding of a kinase-inducible transactivation domain predicts its structure on coactivator binding. *Biochemistry* **37:** 5858–5866.

Hwang, T., van Zijl, P.C.M., and Mori, S. 1998. Accurate quantitation of water–amide proton exchange rates using the phase-modulated CLEAN chemical EXchange (CLEANEX-PM) approach with a Fast-HSQC (FHSQC) detection scheme. *J. Biomol. NMR* **11:** 221–226.

Johnson, B.A. and Blevins, R.A. 1994. NMRView: A computer program for the visualization and analysis of NMR data. *J. Biomol. NMR* **4:** 603–614.

Kordeli, E. 2000. The spectrin-based skeleton at the postsynaptic membrane of the neuromuscular junction. *Microsc. Res. Tech.* **49:** 101–107.

Kusunoki, H., MacDonald, R.I., and Mondragon, A. 2004. Structural insights into the stability and flexibility of unusual erythroid spectrin repeats. *Structure* **12:** 645–656.

Lu, J., Cistola, D.P., and Li, E. 2006. Analysis of ligand binding and protein dynamics of human retinoid X receptor α-ligand-binding domain by nuclear magnetic resonance. *Biochemistry* **45:** 1629–1639.

Mackay, J.P., Shaw, G.L., and King, G.F. 1996. Backbone dynamics of the c-Jun leucine zipper: ^{15}N NMR relaxation studies. *Biochemistry* **35:** 4857–4877.

Mehboob, S., Luo, B., Patel, B.M., and Fung, L.W. 2001. αβ Spectrin coiled coil association at the tetramerization site. *Biochemistry* **40:** 12457–12464.

Mehboob, S., Jacob, J., May, M., Kotula, L., Thiyagarajan, P., Johnson, M.E., and Fung, L.W. 2003. Structural analysis of the α N-terminal region of erythroid and nonerythroid spectrins by small-angle X-ray scattering. *Biochemistry* **42:** 14702–14710.

Mehboob, S., Luo, B., Fu, W., Johnson, M.E., and Fung, L.W.-M. 2005. Conformational studies of the tetramerization site of human erythroid spectrin by cysteine-scanning spin-labeling EPR methods. *Biochemistry* **44:** 15898–15905.

Pace, C.N. and Scholtz, J.M. 1998. A helix propensity scale based on experimental studies of peptides and proteins. *Biophys. J.* **75:** 422–427.

Park, S., Liao, X., Johnson, M.E., and Fung, L.W.-M. 1999. ^{1}H, ^{15}N, and ^{13}C NMR backbone assignments of the N-terminal region of human erythrocyte α spectrin including one structural domain. *J. Biomol. NMR* **15:** 345–346.

Park, S., Johnson, M.E., and Fung, L.W.-M. 2000. NMR analysis of secondary structure and dynamics of a recombinant peptide from the N-terminal region of human erythroid α-spectrin. *FEBS Lett.* **485:** 81–86.

Park, S., Johnson, M.E., and Fung, L.W.-M. 2002. Nuclear magnetic resonance studies of mutations at the tetramerization region of human α spectrin. *Blood* **100:** 283–288.

Park, S., Caffrey, M.S., Johnson, M.E., and Fung, L.W.-M. 2003. Solution structural studies on human erythrocyte α-spectrin tetramerization site. *J. Biol. Chem.* **278:** 21837–21844.

Pervushin, K., Riek, R., Wider, G., and Wüthrich, K. 1997. Attenuated T_2 relaxation by mutual cancellation of dipole–dipole coupling and chemical shift anisotropy indicates an avenue to NMR structures of very large biological macromolecules in solution. *Proc. Natl. Acad. Sci.* **94:** 12366–12377.

Salomao, M., An, X., Guo, X., Gratzer, W.B., Mohandas, N., and Baines, A.J. 2006. Mammalian α I-spectrin is a neofunctionalized polypeptide adapted to small highly deformable erythrocytes. *Proc. Natl. Acad. Sci.* **103:** 643–648.

Speicher, D.W. and Marchesi, V.T. 1984. Erythrocyte spectrin is comprised of many homologous triple helical segments. *Nature* **311:** 177–180.

Speicher, D.W., DeSilva, T.M., Speicher, K.D., Ursitt, J.A., Hembach, P., and Weglarz, L. 1993. Location of the human red cell spectrin tetramer binding site and detection of a related ''closed'' hairpin loop dimer using proteolytic footprinting. *J. Biol. Chem.* **268:** 4227–4235.

Tanahatoe, J.J. and Kuil, M.E. 1997. Molar mass dependence of the apparent diffusion coefficient of flexible highly charged polyelectrolytes in the dilute concentration regime. *J. Phys. Chem. A* **101:** 8389–8394.

Ursitti, J., Kotula, L., DeSilva, T.M., Curtis, P.J., and Speicher, D.W. 1996. Mapping the human erythrocyte β-spectrin dimer initiation site using recombinant peptides and correlation of its phasing with the α-actinin dimer site. *J. Biol. Chem.* **271:** 6636–6644.

Uversky, V.N. 2002. Natively unfolded proteins: A point where biology waits for physics. *Protein Sci.* **11:** 739–756.

Yan, Y., Winograd, E., Viel, A., Cronin, T., Harrison, S.C., and Branton, D. 1993. Crystal structure of the repetitive segments of spectrin. *Science* **262:** 2027–2030.